Redox Biology 61 (2023) 102649

Contents lists available at ScienceDirect

Redox Biology

journal homepage: www.elsevier.com/locate/redox

Genistein mitigates senescence of bone marrow mesenchymal stem cells via ERRα-mediated mitochondrial biogenesis and mitophagy in ovariectomized rats

Mengyu Li [a,1], Yejia Yu [a,1], Ke Xue [b,1], Jiayi Li [a], Geehun Son [a], Jiajia Wang [a], Wentao Qian [a], Shaoyi Wang [a], Jiawei Zheng [c], Chi Yang [a,**], Jing Ge [a,*]

[a] Department of Oral Surgery, Shanghai Ninth People's Hospital, Shanghai Jiao Tong University School of Medicine, College of Stomatology, Shanghai Jiao Tong University, National Center for Stomatology, National Clinical Research Center for Oral Diseases, Shanghai Key Laboratory of Stomatology, Shanghai Research Institute of Stomatology, Shanghai, China

[b] Department of Pastic and Reconstructive Surgery, Shanghai Ninth People's Hospital, Shanghai Jiao Tong University School of Medicine, Shanghai, China

[c] Department of Oromaxillofacial Head and Neck Surgery, Shanghai Ninth People's Hospital, Shanghai Jiao Tong University School of Medicine, College of Stomatology, Shanghai Jiao Tong University, National Center for Stomatology, National Clinical Research Center for Oral Diseases, Shanghai Key Laboratory of Stomatology, Shanghai Research Institute of Stomatology, Shanghai, China

ARTICLE INFO

Keywords:
Mesenchymal stem cells
Senescence
Mitophagy
Estrogen-related receptor α
Osteoporosis

ABSTRACT

Senescence of bone marrow mesenchymal stem cells (BMMSCs) induced by chronic oxidative stress is an important factor contributes to the postmenopausal osteoporosis (PMOP). Mitochondrial quality control takes a pivotal role in regulating oxidative stress and cell senescence. Genistein is a major isoflavone in soy products, which is best known for its ability to inhibit bone loss in both postmenopausal women and ovariectomized (OVX) rodents. Here we show that OVX-BMMSCs displayed premature senescence, elevated reactive oxygen species (ROS) level and mitochondria dysfunction, while genistein rescued these phenotypes. Using network pharmacology and molecular docking, we identified estrogen-related receptor α (ERRα) as the potential target of genistein. Knockdown of ERRα greatly abolished the anti-senescence effect of genistein on OVX-BMMSCs. Further, the mitochondrial biogenesis and mitophagy induced by genistein were inhibited by ERRα knockdown in OVX-BMMSCs. In vivo, genistein inhibited trabecular bone loss and $p16^{INK4a}$ expression, upregulated sirtuin 3 (SIRT3) and peroxisome proliferator-activated receptor gamma coactivator one alpha (PGC1α) expression in the trabecular bone area of proximal tibia in OVX rats. Together, this study revealed that genistein ameliorates senescence of OVX-BMMSCs through ERRα-mediated mitochondrial biogenesis and mitophagy, which provided a molecular basis for advancement and development of therapeutic strategies against PMOP.

1. Introduction

Postmenopausal osteoporosis (PMOP) is a systemic skeletal disorder characterized by low bone mass and increased fracture risk, which is triggered by estrogen deficiency during menopause [1]. Premature senescence of stem cells is recognized as a critical pathogenesis of bone deteriorations in PMOP [2]. Mechanistically, mitochondrial dysfunctions, in particular bioenergetic decline and reactive oxygen species (ROS) accumulation, are crucial mechanisms underlying stem cell senescence. Accordingly, approaches aimed at restoring mitochondrial homeostasis may provide promising opportunities to counteract PMOP [3].

Mitochondrial homeostasis is a sophisticated regulatory network that coordinates various cellular pathways, including the interplay between mitochondrial biogenesis and mitophagy. The tight coordination of these two opposing processes preserves mitochondrial function and

* Corresponding author. Department of Oral Surgery, Shanghai Ninth People's Hospital, College of Stomatology, Shanghai Jiao Tong University School of Medicine, Shanghai Key Laboratory of Stomatology & Shanghai Research institute of Stomatology, Shanghai, China.

** Corresponding author. Department of Oral Surgery, Shanghai Ninth People's Hospital, College of Stomatology, Shanghai Jiao Tong University School of Medicine, Shanghai Key Laboratory of Stomatology & Shanghai Research institute of Stomatology, Shanghai, China.

E-mail addresses: yangchi63@hotmail.com (C. Yang), 2044328567@qq.com (J. Ge).

[1] Mengyu Li, Yejia Yu and Ke Xue contributed equally to this work.

https://doi.org/10.1016/j.redox.2023.102649
Received 2 February 2023; Received in revised form 25 February 2023; Accepted 25 February 2023
Available online 27 February 2023

cell homeostasis. Mitochondrial biogenesis provides the cell with newly synthesized mitochondria, thus preserves mitochondrial function and cellular homeostasis. Inhibition of mitochondrial biogenesis can lead to defective osteogenesis of bone marrow mesenchymal stem cells (BMMSCs) [4]. Besides mitochondrial biogenesis, degradation of defective or superfluous mitochondria through mitophagy process also serves as another machinery for the maintenance of mitochondrial integrity and quality control [5]. Defective mitophagy can lead to accumulation of damaged mitochondria [6], which generate inefficient oxidative phosphorylation and further increases ROS production. Induction of mitophagy alleviates the damage caused by oxidative stress [7]. Therefore, restoring the mitochondrial homeostasis of BMMSCs is possibly an effective method to against PMOP.

Genistein, the principal soy phytoestrogen, has been proved to prevent bone loss in postmenopausal women [8] and ovariectomized (OVX) rodents [9,10]. It was reported that genistein could mitigate mitochondrial dysfunctions in many pathological conditions, including neuroinflammation and aggregation of Aβ in Alzheimer's disease [11]. Therefore, it is likely that genistein exert anabolic effect partially through modulating mitochondrial homeostasis to reduce oxidative stress, thus reverse premature senescence of OVX-BMMSCs during estrogen deficiency.

In the present study, we systematically characterized the role of genistein in regulating the senescence of BMMSCs during estrogen deficiency. We determined that OVX-BMMSCs presented premature senescence phenotype compared to the Sham-BMMSCs, and genistein treatment greatly ameliorated cellular senescence in OVX-BMMSCs. Using integrated bioinformatic analysis, we identified estrogen-related receptor α (ERRα) as the potential target of genistein in PMOP. Remarkably, genistein-induced mitochondria biogenesis and mitophagy were largely prevented by transfection of ERRα siRNA. As a result, the anti-senescence effect of genistein in OVX-BMMSCs was abolished by ERRα knockdown. Collectively, these data demonstrate genistein exert anti-senescence effect on OVX-BMMSCs by restoring mitochondrial homeostasis in an ERRα-dependent manner, which provide further evidence for its use as a natural therapeutic agent for PMOP. It also suggested that the agonists of ERRα may be a viable therapeutic strategy to preserve bone mass in PMOP.

2. Materials and methods

2.1. Cell culture and reagents

Twelve-week-old female Sprague-Dawley rats were subjected to either bilateral ovariectomy or sham surgery. Briefly, rats were anaesthetized and the bilateral ovaries were gently removed via a dorsal approach. For the Sham group, animals received the operation without removing the ovaries. Sixteen weeks after surgery, Sham-BMMSCs and OVX-BMMSCs were harvested from the bone marrow of the tibias and femurs from Sham rats and OVX rats, respectively. Sham-BMMSCs were maintained in DMEM medium plus 10% FBS (Gibco, Grand Island, NY, USA) and 1% penicillin-streptomycin (Gibco). OVX-BMMSCs were cultured in the same condition except that the DMEM medium is phenol red free (Gibco) to mimic the environment in vivo. Genistein and N-acetylcysteine (NAC) were obtained from Sigma (Sigma-Aldrich Inc., St. Louis, MO, USA) and bafilomycin A1 (Baf-A1) was purchased from CST (Cell Signaling Technology, Beverly, MA, USA). NAC is a classic antioxidant that is well known for its ability to minimize intracellular oxidative stress. Baf-A1, a vacuolar-type H^+-translocating ATPase (V-ATPase) inhibitor, was used as an autophagy inhibitor as it blocks the fusion of autophagosomes with lysosomes [12].

Antibodies were from various sources, including Abcam (anti-$p21^{CIP1}$, anti-TOM20, anti-PGC1α, anti-LC3B, anti-P62, HRP-conjugated goat anti-rabbit and FITC-conjugated goat anti-rabbit), CST (anti-p53, anti-CoxIV, anti-γH2AX, anti-β-actin, HRP-conjugated anti-rabbit and HRP-conjugated anti-mouse), Invitrogen (anti-$p16^{INK4a}$, anti-SIRT3 and anti-LepR), and Proteintech (anti-PGC1α and anti-Parkin).

2.2. Phenotypic characterization

For phenotypic characterization, cells were stained with fluorochrome-conjugated monoclonal antibodies including CD45-FITC (Elabscience, E-AB-F1227C), CD31-FITC (Abcam, ab33858), CD90-FITC (Elabscience, E-AB-F1226C) and CD44-FITC (Elabscience, E-AB-F1225C). Corresponding mouse IgG1-FITC (Elabscience, E-AB-F09792C) and mouse IgG2a-FITC (Elabscience, E-AB-F09802C) were used as isotype control. The samples were incubated for 30 min in the dark and then washed for 2 times. All samples were resuspended in 500 μl PBS and analyzed by flow cytometer (Beckman, CytoFLEX LX) and FlowJo software (Version 10.8.1, Tree Star, San Carlos, CA).

2.3. Small interfering RNA (siRNA) transfection

ERRα siRNAs and negative control (NC) siRNAs were purchased from HanBio Technology Company (Shanghai, China) and the transfection was carried out according to the manufacturer's instruction. Briefly, cells were seeded in 6-well plate using growth medium without antibiotic one day before transfection. ERRα siRNA or NC siRNA were premixed with Lipofectamine RNAiMAX (Invitrogen) and then added into the cell medium with the final siRNA concentration of 100 nM. After 48-h incubation, the transfection medium was changed with fresh medium with or without genistein. The protein expression of ERRα in cells transfected with siRNA was examined by western blot analysis. The sequences of rat siRNA are as follows:

ERRα: 5'- GGCCUCCAAUGAGUGUGAGAU-3';

Scrambled siRNA: 5'-UUCUCCGAACGUGUCACGU-3'.

2.4. Cell viability assay

Cell viability was evaluated by cell counting kit-8 (Dojindo, Japan). Briefly, 3×10^3 cells were plated in 96 well plates and were incubated with various concentrations of genistein for 24 h, 48 h and 72 h. After treatment, cells were incubated in 10% CCK-8 reagent for another 2 h. The optical density (OD) value was measured at 450 nm with a microplate reader (ELx800; BioTek Instruments, USA).

2.5. Colony-forming assays

Cells (300 cells/well) were seeded into 6-well plates and cultured in conditioned medium for 10 days. Cells were fixed in 4% paraformaldehyde (m/v) for 15min at room temperature (RT). After rinsing with PBS, cells were stained with crystal violet solution (Sigma). The images were captured by microscope and the colonies (aggregates≥50 cells) were counted.

2.6. Senescence β-galactosidase (β-Gal) staining

To assess cell senescence, β-Gal activity was determined by using β-Gal Staining Kit (Beyotime, Institute of Biotechnology, China). Briefly, cells were fixed in fixation buffer for 15 min at RT, then washed and incubated with staining solution at 37 °C overnight. The number of blue cells positive for SA-β-Gal was expressed as % of total cell number (100 cells counted for each condition, three independent experiments).

2.7. Immunofluorescence staining

Cells were seeded onto gelatin-coated glass slides and treated with conditioned medium for 48 h. After removing the medium, the cells were fixed with 4% paraformaldehyde for 20 min, permeabilized with 0.2% Triton X-100 for 10min, and then blocked with goat serum for 1 h. For protein detection and localization, the cells were incubated with specific primary antibodies (anti-γH2AX, 1:400; anti-Parkin, 1:200; anti-

TOM20, 1:200) overnight. All samples were then washed 3 times and incubated with fluorescent secondary antibody (1:1000, Abcam) for 2 h. DAPI was used for nucleus counter staining. The photographs were acquired by using a Nikon fluorescence microscope. The γH2AX intensity was divided by the DAPI intensity. Three random fields of view were included into the measurement for each slide, and the assays were repeated for three biological replicates.

2.8. Mitochondrial DNA copy number assay

Mitochondrial DNA (mtDNA) copy number was determined by quantitative real-time PCR as described [13]. Briefly, total DNA was extracted and purified from cells using a DNeasy Blood & Tissue kit (Qiagen, Hilden, Germany). Quantification of mtDNA was performed by use of the ratio of mtDNA marker mitochondrial NADH dehydrogenase 1 (mt-ND1) (Forward: 5′-CGTTGCCCAAACCATCTCT-3′, Reverse: 5′-CTATTGGTCAGGCGGGGA-3′) to nuclear DNA marker β-actin (Forward: 5′- TTGTCACCAACTGGGACGATATGG-3′, Reverse: 5′-GGGGTGTTGAAGGTCTCAAACATG-3′). The relative mtDNA copy number was measured by normalization of the crossing points in quantitative PCR curves between ND1 and β-actin genes using the RelQuant software (Roche Applied Sciences).

2.9. ROS measurements

Cellular ROS level was measured by a DCFDA fluorescent probe (Beyotime). Briefly, cells were wash with HBSS twice and incubated with serum-free DMEM containing 10 μM DCFDA at 37 °C for 20 min. The photographs were captured by a Nikon fluorescence microscope. ROS generation was determined by using a FACSCalibur flow cytometer (Beckman, CytoFLEX LX). The data from flow cytometry were analyzed using FlowJo software, and mean fluorescence intensity (MFI) in each group was recorded and analyzed. When indicated, 5 mM NAC was used as an antioxidant positive control.

2.10. Mitochondrial superoxide Quantification

Cells were incubated with 5 μM MitoSOX Red (Invitrogen) for 10 min, then washed with warm HBSS to remove the excess dye. To visualize the stained cells, random fields in each group were captured by using a Nikon fluorescence microscope. To quantify the MitoSOX Red fluorescence intensity, cells were collected and sorted by FACSCalibur flow cytometer (Beckman). The data from flow cytometry were analyzed using FlowJo software, and the mean fluorescence intensity (MFI) in each group was recorded and analyzed.

2.11. ATP content and mitochondrial membrane potential detection

ATP content of cells was determined with the ATP assay kit (Abcam, ab83355) according to manufacturer's protocol. Briefly,1×10^6 cells were resuspended in 100 μL of ATP assay buffer, then homogenized and centrifuged for 5 min at 4 °C. The supernatant was collected and added to plate at 50 μL/well. Add 50 μL ATP reaction mix to each well, incubate the plate at room temperature for 30 min, then measure output on a microplate reader at OD 570 nm. Subtract the mean value of the blank from all standards and sample readings. The sample values were calculated from the standard curve and normalized to the control group in each individual experiment.

For measuring mitochondrial membrane potential, a JC-1 kit (Beyotime) was used. JC-1 is cationic dye that exhibit potential-dependent accumulation in mitochondria, indicated by a fluorescence emission shift from green to red. Mitochondrial depolarization is indicated by a decrease in the red/green fluorescence intensity ratio. Cells were incubated with JC-1 dye for 20 min at 37 °C in the dark. Thereafter, cells were either assessed by fluorescence microscope or harvested and analyzed by flow cytometry. The data from flow cytometry were analyzed using FlowJo software, and median PE and FITC fluorescence were used to calculate a red/green ratio as an index of mitochondrial membrane potential [14].

2.12. Oxygen consumption rate (OCR)

The measurement of OCR in cells were performed using Seahorse XF96 analyzer (Agilent Technologies, Santa Clara, CA) following manufacturer's protocol. Briefly, OVX-BMMSCs were plated at density of 10,000 cells/well in a Seahorse cell culture microplate and transfected with siNC/siERRα. After 48 h transfection, the media is replaced with culturing medium with/without genistein for another 72 h. On the day of measurement, the medium was changed to pre-warmed Seahorse assay medium, and OCR determined using the Seahorse XF Cell Mito Stress Kit (Agilent). After recording 3 total cellular respiration measurements in unstimulated cells, oligomycin (1.5 μM) was added to inhibit mitochondrial ATP synthase and measure the decrease in the OCR that is linked to ATP turnover. To determine the maximal respiration potential of the cells, FCCP (1 μM; an uncoupler of oxidative phosphorilation) was used. The amount of nonmitochondrial oxygen consumption was determined by inhibiting the respiratory chain activity with antimycin A and rotenone cocktail (0.5 μM). After completion, cells were lysed with RIPA buffer (Beyotime), and OCR was normalized to protein content determined using a BCA protein assay kit (Beyotime) according to the manufacturer's instructions.

2.13. Transmission electron microscopy (TEM) analysis

Cells were washed with PBS (PH 7.4) and primarily fixed in 2.5% glutaraldehyde for 24 h. The samples were post-fixed in 1% OsO_4 for 1 h at RT, then progressively dehydrated through graded ethanol/acetone solutions and embedded in epoxy resin. Finally, ultrathin sections (70 nm) were prepared and stained with 2% uranyl acetate followed by lead citrate. The images of cell ultrastructure were captured with a transmission electron microscope (JEOL, Tokyo, Japan). The experiments were repeated for three biological replicates.

2.14. Live cell imaging microscopy

Cells were loaded with green-fluorescing mitochondrial dye MitoTracker Green (MTG, 20 nM) (Invitrogen) for 30min at 37 °C, then washed 2 times with fresh complete growth medium and incubated with red-fluorescing LysoTracker Red (LTR, 50 nM) (Invitrogen) for 30min at 37 °C. After MTG and LTR had been loaded, confocal images were acquired by using a confocal laser scanning microscope (TCS SP8, Leica Microsystems, Germany). MTG was excitated at 490/516 nm and LTR was excitated at 577/590 nm. Co-localization of both signals is counted as a mitophagy event. The Pearson's colocalization coefficient between MTG and LTR fluorescence intensities was determined in 9 cells from three independent experiments using Image J software [13].

For functional mitochondria staining, cells were loaded with MitoTracker Red CMXRos (MTR, 20 nM) (Invitrogen) for 30min at 37 °C, then washed 2 times with fresh complete growth medium. Confocal images were acquired by using a confocal laser scanning microscope (Leica). MTR was excitated at 579/599 nm. The stained cells were also sorted by FACSCalibur flow cytometer (Beckman). The data from flow cytometry were analyzed using FlowJo software, and the mean fluorescence intensity (MFI) in each group was recorded and analyzed.

2.15. Total RNA extraction and quantitative real-time PCR analysis

Targeted gene expression analyses were performed by rt-qPCR as described [15]. Briefly, total RNA was extracted with Trizol reagent (Invitrogen, Carlsbad, CA), followed by cDNA synthesis using Reverse Transcription Kit (TaKaRa, Japan) according to the manufacturer's instructions. qRT-PCR were performed on a Roche Light Cycler 480

(Roche, Mannheim, Germany) using the SYBR Green PCR Master Mix (TaKaRa, Japan). Fold changes of mRNA were calculated by the $2^{-\Delta\Delta}$Ct method after normalization to the expression of β-actin (ACTB). Sequences of the primers are listed in Supplementary Table S1.

2.16. Western blotting

The cells were dissociated with RIPA buffer (Beyotime) containing protease inhibitor and phosphatase inhibitors (Sigma). After concentration measurement, 20 μg of protein was loaded onto 4–20% SDS-PAGE gel and transferred to a PVDF membrane (Millipore, Billerica, MA, USA). The membrane was blocked by 5% non-fat milk for 2 h followed by incubated with primary antibody at 4 °C overnight. Subsequently, the blots were incubated for 1 h at RT with an HRP-conjugated secondary antibody (CST), and visualized by chemiluminescence detection system (Millipore). Quantitative analysis of the Western blot was carried out by using Image J software, and band intensity was normalized to β-actin.

The primary antibodies used were, anti-$p21^{CIP1}$ (1:1000, Abcam, ab109199) anti-TOM20 (1:1000, Abcam, ab186735), anti-PGC1α (1 μg/ml, Abcam, ab106814), anti-LC3B (1:2000, Abcam, ab192890), anti-P62 (1:1000, Abcam, ab56416), anti-p53 (1:1000, CST, #2524), anti-CoxIV (1:1000, CST, #4850), anti-β-actin (1:1000, CST, #8457), and anti-SIRT3 (1:1000, Invitrogen, PA5-96406).

2.17. Drug-target interaction prediction

Drug–target network (DTN) from genistein and targets associations in postmenopausal osteoporosis was constructed and analyzed by the DrugBank 4.0 database. Then, we mapped the primary target proteins into the online STRING database to generate protein-protein interaction (PPI) network generation. Interaction pairs with overall score above 0.9 were recorded. To characterize the biochemical pathways and functions linked to genistein, GO (Gene Ontology) enrichment analysis and KEGG (Kyoto Encyclopedia of Genes and Genomes) pathway enrichment analysis were carried out.

2.18. Molecular docking analysis

The chemical structure of genistein was obtained from the PubChem database, and genistein were imported into Schrodinger for 3D format conversion and energy minimization. The protein structure of ERRα was obtained by SwisS-Model online server and processed in Maestro11.9. Schrodinger's Protein Preparation Wizard was used to process the protein structure, remove the crystal water, replenish the missing hydrogen atoms, repair the missing bond information, repair the missing peptide, and finally minimize the energy of the Protein [16,17]. Then, Molecular docking studies using ERRα with genistein was performed by the Glide module in Schrodinger Maestro software. Finally, the screening and analysis of docking results were carried out by SP.

2.19. Animals and drug treatment

All animal protocol was critically reviewed and approved by the institutional review board of Shanghai Jiao Tong University School of Medicine (institutional review board no. SH9H-2020-A704-1). This study conformed to the ARRIVE (Animal Research: Reporting In Vivo Experiments) guidelines for animal studies.

A total of 60 female Sprague-Dawley rats, mean weight 220 ± 25 g, were obtained at 3-month of age from the Ninth People's Hospital Animal Center (Shanghai, China). Rats were maintained under the following environmental conditions: temperature: 25 ± 3 °C; humidity: 50 ± 10%; illumination: light/dark cycle 12/12; free access to water and a diet low in phytoestrogen content. Following 2 weeks of adaptation, 30 rats were received operation to establish the OVX-OP model and 30 rats were received sham operation.

Eight weeks after surgery, rats received the following treatments with 15 rats in each group: (1) Sham + VEH group: oral saline solution treatment once daily; (2) Sham + GEN group: oral genistein (50 mg/kg body weight, Sigma-Aldrich, MO, USA) treatment once daily. (3) OVX + VEH group: oral saline solution treatment once daily; (4) OVX + GEN group: oral genistein (50 mg/kg body weight) treatment once daily.

After being fed for 8 weeks, blood was withdrawn before the rats were sacrificed, and serum was then prepared. Rats were sacrificed by cervical dislocation under halothane anesthesia. Femurs and tibias were collected for further analysis.

2.20. Measurement of serum MDA

The activity of MDA in serum was measured by using a lipid peroxidation MDA assay kit (Beyotime) according to the manufacturer's instructions. Briefly, the serum was incubated with reagent in each reaction tube at 100 °C for 15 min. After centrifuged at 4000 rpm for 10 min, the supernatants were collected and measured for absorbance at 532 nm with a microplate reader.

2.21. Bone biomechanical test

The femurs were stored frozen at −20 °C before biomechanical test. After thawing, the right femur mid-shaft was taken for the three-point bending assay by using electronic universal testing machine (Shenzhen Reger Instrument Co. Ltd., China) according to Ma et al.'s [18] description. A load was vertically applied to the femoral mid-shaft, with a displacement speed of 0.1 mm/s and span distance at 20 mm until the femoral shaft is fractured. The left femoral neck was tested by mounting the proximal half of the femur vertically in a chuck and applying a downward force on the femoral head until failure. The ultimate load of the femurs was recorded and analyzed.

2.22. Micro-computed tomography (Micro-CT)

Micro-CT scanning was performed by using a micro-CT system (μCT-80, Scanco Medical, Bassersdorf, Switzerland) on proximal tibias before decalcification. To visualize the inside of the proximal tibia, two-dimensional (2-D) images at their most central part were obtained. Trabecular bone was selected as region of interests (ROI) and the following parameters of ROI were analyzed: bone mineral density (BMD), bone volume/total volume (BV/TV), trabecular thickness (Tb. Th) and trabecular separation (Tb.Sp).

2.23. Histological analysis

Decalcification of specimens was carried out with 10% EDTA with constant shaking for 8 weeks. After decalcification, the specimens were embedded in paraffin and cut into 5-μm-thick sections. Three sections of the most central part of the proximal tibia were selected and underwent H-E staining. For immunohistochemistry, sections were deparaffinized, rehydrated, and incubated with primary antibody (anti-$p16^{INK4a}$, 5 μg/mL, Invitrogen) at 4 °C overnight after antigen retrieval. The sections were then washed in PBS and incubated with secondary antibody (HRP-conjugated goat anti-rabbit, 1:1000, Abcam), and stained with DAB kit. The sections were observed under a light microscope.

For immunofluorescence staining, sections were incubated with a primary antibody (anti-SIRT3, 1:100, Invitrogen) at 4 °C overnight and then with a secondary antibody (FITC-conjugated goat anti-rabbit, 1:1000, Abcam) for 1 h at 37 °C. Afterwards, slides were stained with DAPI and mounted with an anti-fade reagent (Invitrogen). Confocal images of slides were obtained by using a confocal microscope (Leica).

For peroxisome proliferator-activated receptor gamma coactivator one alpha (PGC1α) and leptin receptor (LepR) immunofluorescence staining, sections were blocked with 10% goat serum (Gibco) and then incubated with primary antibodies (anti- PGC1α, 1:50, Proteintech; anti-

LepR, 1:50, Invitrogen) at 4 °C overnight and with secondary antibodies for 1 h at 37 °C. Slides were then stained with DAPI and mounted with an anti-fade reagent (Invitrogen). The images were captured by a Zeiss LSM710 confocal microscope (Carl Zeiss).

Image J software was used for quantification of IHC and IF. For quantification of $p16^{INK4a}$ staining, three random fields of view per specimen were taken, and the average values were taken as the data point for each specimen. The SIRT3 intensity was divided by the DAPI intensity, and the PGC1α intensity was divided by the LepR intensity. Three random fields of view were included into the measurement for each specimen, and nine specimens in each group were selected for immunohistochemistry and immunofluorescence staining. All data was analyzed blinded.

2.24. Statistical analysis

Data were presented as means ± SD. At least three samples or independent experiments were performed with all the assays. All statistical analyses were performed using the GraphPad prism (Version 9.0, GraphPad Software, San Diego, CA). Normal distribution of the data was verified using Shapiro-Wilk test and the equality of variances was verified by Levene's test. P values were calculated by unpaired Student's *t*-test, or one-way ANOVA for samples following normal distribution. For ANOVA, Tukey's post-test was used to compare individual groups. Mann-Whitney, or Kruskal-Wallis tests were used when samples didn't follow a normal distribution. For Kruskal-Wallis test, Dunn's multiple comparisons test was used for post-hoc analysis. P value < 0.05 was taken as statistical significance.

3. Results

3.1. Genistein alleviated the senescence of OVX-BMMSCs

Primary cultured BMMSCs were positive for surface markers (CD44 and CD90) and negative for hematopoietic cell markers (CD31 and CD45) (Fig. 1A). Cell viability assay showed that genistein had no cell toxicity when used at concentrations ranging from 10^{-3} to 1 μM (Fig. 1B). The expression of phosphorylated H2A histone family member X (γH2AX), a marker of DNA damage, was upregulated in the OVX-BMMSCs versus Sham-BMMSCs (Fig. 1C and D). Consistently, OVX-BMMSCs displayed senescence phenotype, as shown by the reduced colony forming ability (Fig. 1E and F) and increased SA-β-gal positive cells (Fig. 1E, G). Then, we explored the effect of genistein on senescence of OVX-BMMSCs at concentration of 1 μM and 10^{-2}μM, as these concentrations have been identified as the optimal concentrations in previous study [19]. Administration of genistein could increase the number

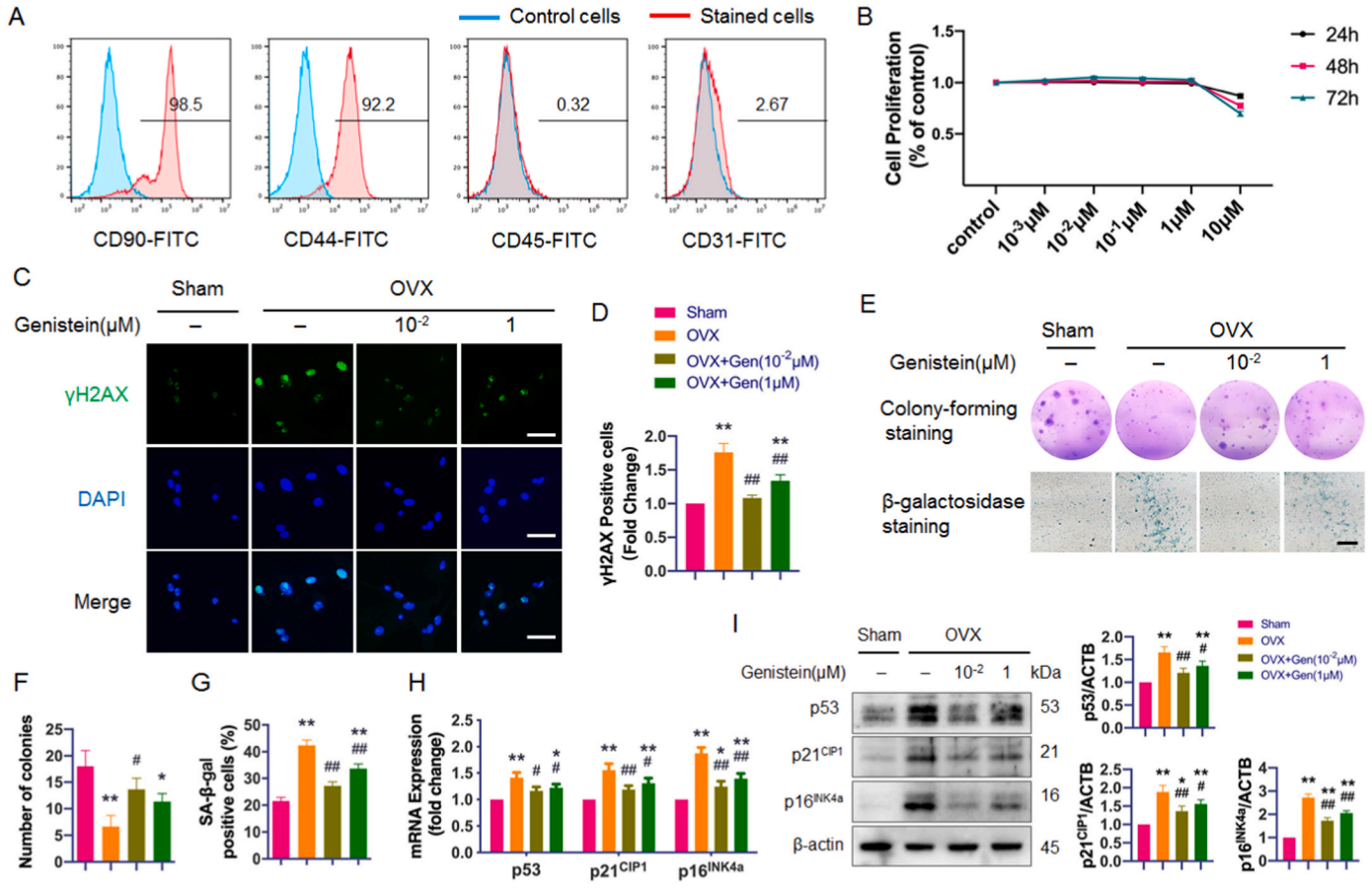

Fig. 1. Genistein alleviated cellular senescence of OVX-BMMSCs. (A) Flow cytometric analysis for cell surface markers of rat BMMSCs (n = 3). (B) Cell viability assay of cells treated by escalating doses of genistein (0–10 μM) for 24 h, 48 h, and 72 h (n = 3). (C, D) Representative images of γH2AX staining and quantitative assessment of the γH2AX positive cells (n = 3). DAPI-labeled nuclei are in blue and γH2AX is stained in green. Cells were treated by genistein for 3 days. Scale bar, 50 μm. (E, F and G) The representative images and quantitative analysis of colony forming assay and SA-β-gal staining (n = 3). Scale bar, 500 μm. (H, I) The mRNA and protein expression of senescence related marker p53, $p16^{INK4a}$ and $p21^{CIP1}$ of Sham-BMMSCs and OVX-BMMSCs. Cells were treated by genistein for 3 days, when indicated. Statistical analysis of expression of each marker was adjusted to β-actin (n = 3). Each value is mean ± SD. Significance was calculated using a one-way ANOVA followed by the Tukey's post-hoc test (B, D, G, H and I). Kruskal-Wallis test followed by Dunn's multiple comparisons test was used for F. *p < 0.05 and **p < 0.01 compared to the Sham group. #p < 0.05 and ##p < 0.01 compared to the OVX group. (For interpretation of the references to color in this figure legend, the reader is referred to the Web version of this article.)

and size of colonies, and downregulate the SA-β-gal and γH2AX positive cells (Fig. 1C–G). We also analyzed the mRNA and protein expressions of senescence related marker [20] p53, $p16^{INK4a}$ and $p21^{CIP1}$, and found that the OVX-induced upregulation of p53, $p16^{INK4a}$ and $p21^{CIP1}$ in BMMSCs were inhibited by genistein treatment (Fig. 1H and I). Collectively, these data indicated that the estrogen-deficiency induced premature senescence could be alleviated by genistein treatment in BMMSCs.

3.2. Genistein attenuated intracellular ROS generation and mitochondrial damage in OVX-BMMSCs

Evidences demonstrated that ROS plays an important role in POMP [21]. Compare to Sham-BMMSCs, we observed an increase of DCFH-DA positive cells in OVX-BMMSCs (Fig. 2A). Genistein treatment significantly reduced the intracellular ROS level (Fig. 2A). The flow cytometry analysis also showed that the mean fluorescent intensity (MFI) of DCFH-DA in OVX-BMMSCs was significantly higher than MFI of Sham-BMMSCs, and genistein treatment effectively downregulated the ROS level in OVX-BMMSCs (Fig. 2B). Consistently, elevated mitochondrial superoxide generation in OVX-BMMSCs was confirmed by flow cytometry showing nearly 1.5-fold higher MitoSOX Red mean fluorescence intensity (MFI) in OVX-BMMSCs versus Sham-BMMSCs, while both genistein and NAC treatment could inhibit the elevated mitochondrial ROS in OVX-BMMSCs (Fig. 2C and D).

Mitochondrial damage was analyzed by JC-1 staining. Loss of mitochondrial membrane potential was indicated by an increase in the number of green fluorescence-stained cells and a decrease in the number of red fluorescence-stained cells in JC-1 staining. The red/green fluorescence ratio of OVX-BMMSCs was significantly lower than the Sham-BMMSCs, indicating that estrogen deficiency led to an apparent loss of mitochondrial transmembrane potential. However, both NAC and genistein treatment could reverse the decline of mitochondrial membrane potential (Fig. 2E and F).

Collectively, these data indicated that genistein downregulated intracellular ROS generation and mitigated mitochondrial damage in OVX-BMMSCs.

3.3. Genistein promotes mitochondrial biogenesis and mitophagy in OVX-BMMSCs

To better understand the regulation of mitochondria turnover in

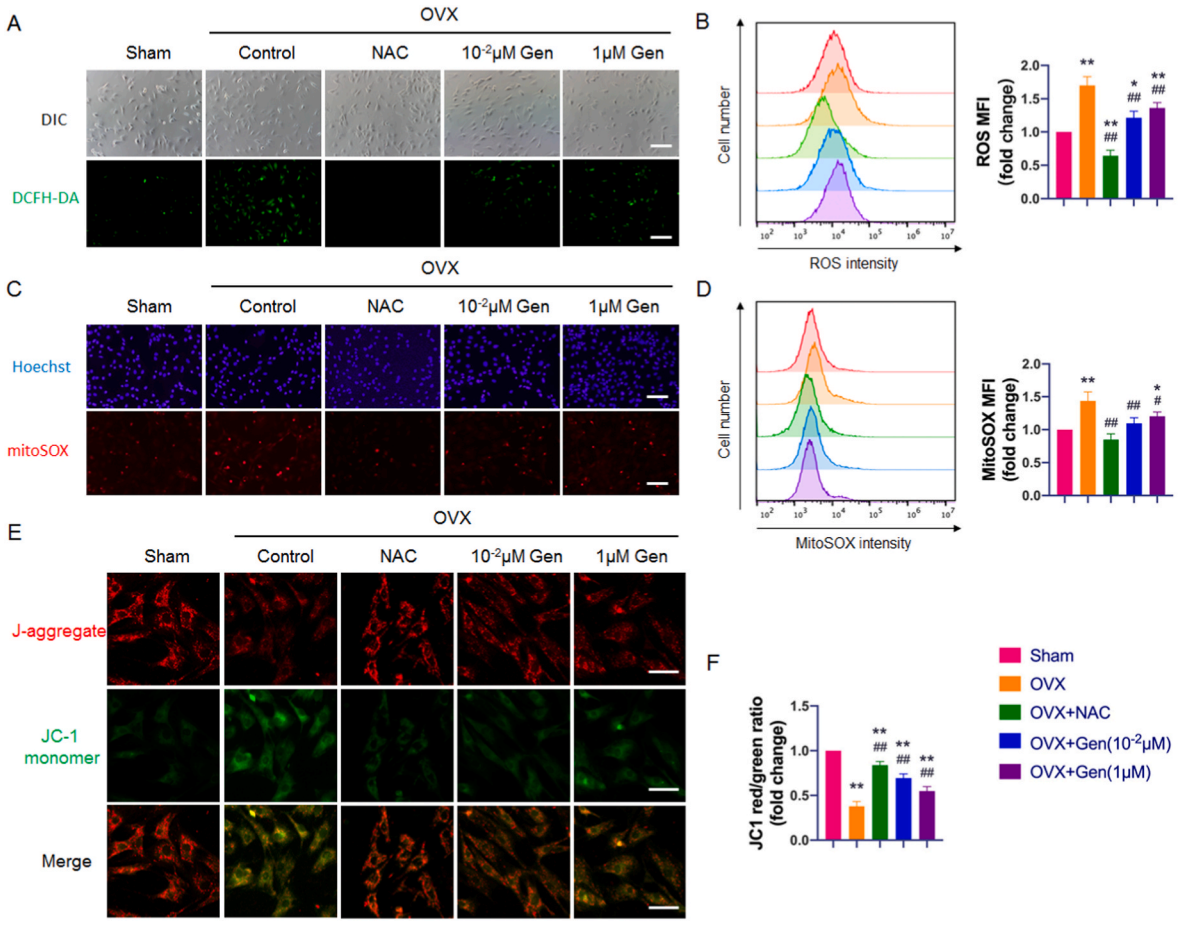

Fig. 2. Genistein attenuated intracellular ROS generation and mitochondrial impairment in OVX-BMMSCs. (A, B) Representative images and flow cytometric analysis of ROS level (n = 3). Cells were treated with different compounds for 3 days as indicated. DIC, differential interference contrast. Scale bar, 200 μm. The mean fluorescent intensity (MFI) of Sham-BMMSCs were normalized to 100%. (C, D) Intracellular superoxide was stained with MitoSOX and detected by flow cytometry (n = 3). The cells were treated with different compounds for 3 days as indicated. The MFI of Sham-BMMSCs were normalized to 100%. (E) Representative images of JC-1 staining. Cells were treated with different compounds for 3 days as indicated. Red fluorescence represented intact mitochondrial membrane potential. Green fluorescence represented reduced mitochondrial membrane potential. Scale bar, 100 μm. (F) Mitochondrial membrane potential measured by JC-1 red/green ratio using flow cytometry (n = 3). The cells were treated with different compounds for 3 days as indicated. The red/green ratio of Sham-BMMSCs were normalized to 100%. Each value is mean ± SD. Significance was calculated using a one-way ANOVA followed by the Tukey's post-hoc test (B, D and F). *$p < 0.05$ and **$p < 0.01$ compared to the Sham group. #$p < 0.05$ and ##$p < 0.01$ compared to the OVX group. (For interpretation of the references to color in this figure legend, the reader is referred to the Web version of this article.)

OVX-BMMSCs, we explored the effect of genistein on mitochondrial biogenesis and mitophagy in OVX-BMMSCs. The expression of mitochondrial membrane proteins, CoxIV and TOM20, were significantly upregulated under genistein treatment in OVX-BMMSCs (Fig. 3A). PGC1α, the master regulator of mitochondrial biogenesis, was also upregulated by genistein treatment in OVX-BMMSCs (Fig. 3A). Consistently, the mRNA expressions of key mitochondrial biogenesis regulators such as PGC1α, Tfam, Nrf1 and Tfb2m, were also increased in genistein-treated OVX-BMMSCs (Fig. 3B). Genistein at 10^{-2} μM significantly restored the ATP content in OVX-BMMSCs (Fig. 3C). Interestingly, although the protein levels of CoxIV and TOM20 were slightly higher in the OVX-BMMSCs compared to the Sham-BMMSCs (Fig. 3A), the protein level of PGC1α and mRNA expressions of mitochondrial biogenesis regulators were lower in the OVX-BMMSCs compared to the Sham-

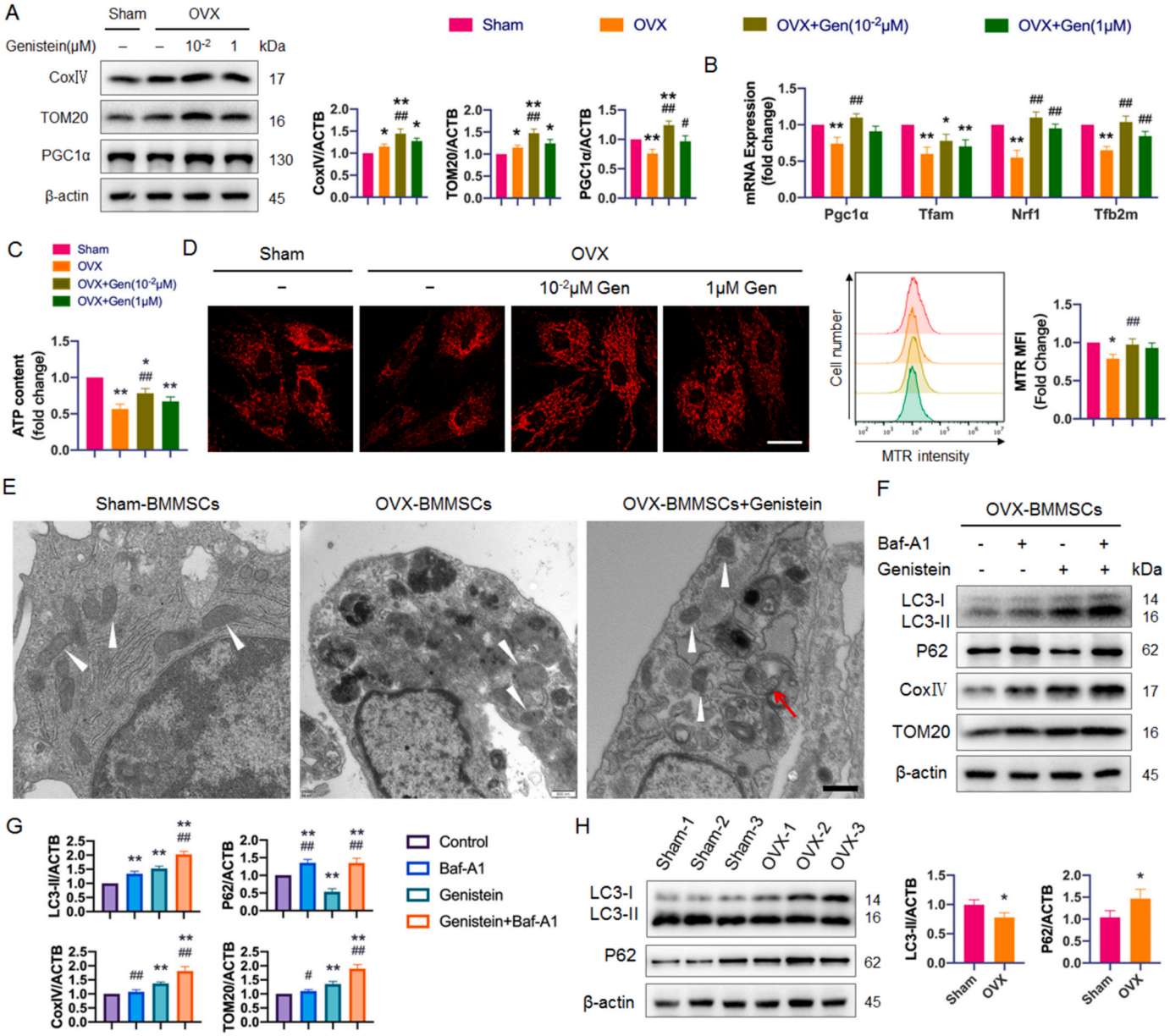

Fig. 3. Genistein promotes mitochondrial biogenesis and mitophagy in OVX-BMMSCs. (A) Protein levels of CoxIV, TOM20 and PGC1α were analyzed by western blots using β-actin as loading control (n = 3). Statistical analysis of expression of CoxIV, TOM20 and PGC1α was adjusted to ACTB. (B) The mRNA expression of Pgc1α, Tfam, Nrf1 and Tfb2m in different groups (n = 3). (C) The ATP level was measured and the values of Sham-BMMSCs were normalized to 100%. (D) Representative images of mitochondria labeled with red (Mito-Tracker Red CMXRos, MTR). The MFI of Sham-BMMSCs were normalized to 100% (n = 3). Cells were treated by genistein for 3 days. Each value is mean ± SD. Significance was calculated using a one-way ANOVA followed by the Tukey's post-hoc test. *p < 0.05 and **p < 0.01 compared to the Sham group. #p < 0.05 and ##p < 0.01 compared to the OVX group. (E) Representative images of transmission electron microscopy (n = 3). OVX-BMMSCs were treated by genistein for 2 days. Mitochondria lost their cristae and formed large vacuoles in OVX-BMMSCs. In Sham-BMMSCs and genistein-treated OVX-BMMSCs, however, mitochondria were intact with clear cristae. Red arrow indicated the mitochondrion was engulfed in an autophagosome, and white arrowheads indicated mitochondria. Scale bar, 500 nm. (F, G) Protein levels of LC3, P62, CoxIV and TOM20 were analyzed by western blots using β-actin as loading control (n = 3). Cells were subjected to indicated treatment for 48 h. Each value is mean ± SD. Significance was calculated using a one-way ANOVA followed by the Tukey's post-hoc test. *p < 0.05 and **p < 0.01 compared to the control group. #p < 0.05 and ##p < 0.01 compared to the genistein group. (H) Protein levels of LC3 and P62 were analyzed by western blots using β-actin as loading control (n = 3). Values represent the mean ± SD of three independent experiments. Significance was calculated using unpaired T-test. *p < 0.05 compared to the Sham group. (For interpretation of the references to color in this figure legend, the reader is referred to the Web version of this article.)

BMMSCs (Fig. 3A and B). Moreover, ATP production was also suppressed in OVX-BMMSCs versus Sham-BMMSCs (Fig. 3C). It raises the question of whether the increased mitochondria in OVX-BMMSCs are dysfunctional.

In order to analyze the content of functional mitochondria, we performed the MitoTracker Red CMXRos (MTR) staining and flow cytometry analysis. MTR is a membrane potential-sensitive probe that can be sequestered by functioning mitochondria. In accordance with the ATP content, the mean fluorescence intensity (MFI) of MTR were significantly lower in the OVX-BMMSCs compared to the Sham-BMMSCs, and 10^{-2} μM genistein treatment increased the functioning mitochondria in OVX-BMMSCs (Fig. 3D). We next performed transmission electron microscopy (TEM) in Sham-BMMSCs, OVX-BMMSCs and OVX-BMMSCs with 10^{-2} μM genistein treatment. The mitochondria in Sham-BMMSCs and genistein-treated OVX-BMMSCs were pristine with intact structures and visible cristae (Fig. 3E, white arrowhead). However, giant mitochondria with aberrant morphology were seen in OVX-BMMSCs (Fig. 3E, white arrowhead). Notably, sequestered mitochondrion in an autophagosome was observed in genistein-treated OVX-BMMSCs, confirming the presence of mitophagy by genistein administration (Fig. 3E, red arrow). To further investigate mitophagy, we used lysosomal inhibitor Baf-A1 to block autophagic clearance of mitochondria. The result of western blot showed slight increase of CoxIV and TOM20 expression in OVX-BMMSCs treated with Baf-A1 (Fig. 3F), indicated that the basal mitophagy was low in OVX-BMMSCs. The impaired mitophagy might account for the increased protein levels of CoxIV and TOM20 in OVX-BMMSCs compared to the Sham-BMMSCs (Fig. 3A), as the cells are unable to remove the dysfunctional mitochondria. Of note, Baf-A1 and genistein (10^{-2}μM) co-treatment could significantly increase the protein levels of CoxIV and TOM20, suggesting that mitophagy was activated by genistein in OVX-BMMSCs (Fig. 3F). Furthermore, the activity of macroautophagy was also impaired in the OVX-BMMSCs (Fig. 3H).

Together, our data demonstrated that genistein at 10^{-2}μM activated mitochondrial biogenesis and mitophagy in OVX-BMMSCs, and we used 10^{-2}μM genistein in the following experiments.

3.4. Molecular docking result of target protein ERRα and genistein in postmenopausal osteoporosis

Next, we used network pharmacology approach and molecular docking to investigate the target of genistein in OVX-BMMSCs. The 11 proteins which identified as primary genistein targets in postmenopausal osteoporosis are ESR2, PTK2B, NCOA1, ESR1, NCOA2, ESRRA, ESRRB, NR1I2, AKT1, CYP1B1 and SHBG. We made the PPI network of the 11 primary protein targets with visualization of genistein target-protein interactions (Fig. 4A). Then, we applied the KEGG biochemical pathways (Fig. 4B) and GO enrichment analysis (Fig. 4C) to assess the functions of genistein-mediated gene sets. Estrogen-related receptor α (ERRα; also known as ESRRA), a member of orphan nuclear hormone receptors, plays an important role in mitochondrial activity [22]. The results of molecular docking showed that genistein had a good binding effect with high matching degree with ERRα (docking score < -5 kcal/mol). The complex formed by docked compound and protein was visualized by Pymol2.1 software. According to the binding mode, amino acid residues combining compound and protein pocket could be clearly seen (Fig. 4D–F).

3.5. Genistein attenuated senescence and mitochondrial dysfunction via ERRα

Since ERRα plays an important role in mitochondrial biogenesis and mitophagy, we wondered whether the anti-senescence effect of genistein was depend on ERRα. As shown in Fig. 5A and B, the downregulation effect on mRNA and protein expression of p53, $p16^{INK4a}$ and $p21^{CIP1}$ by

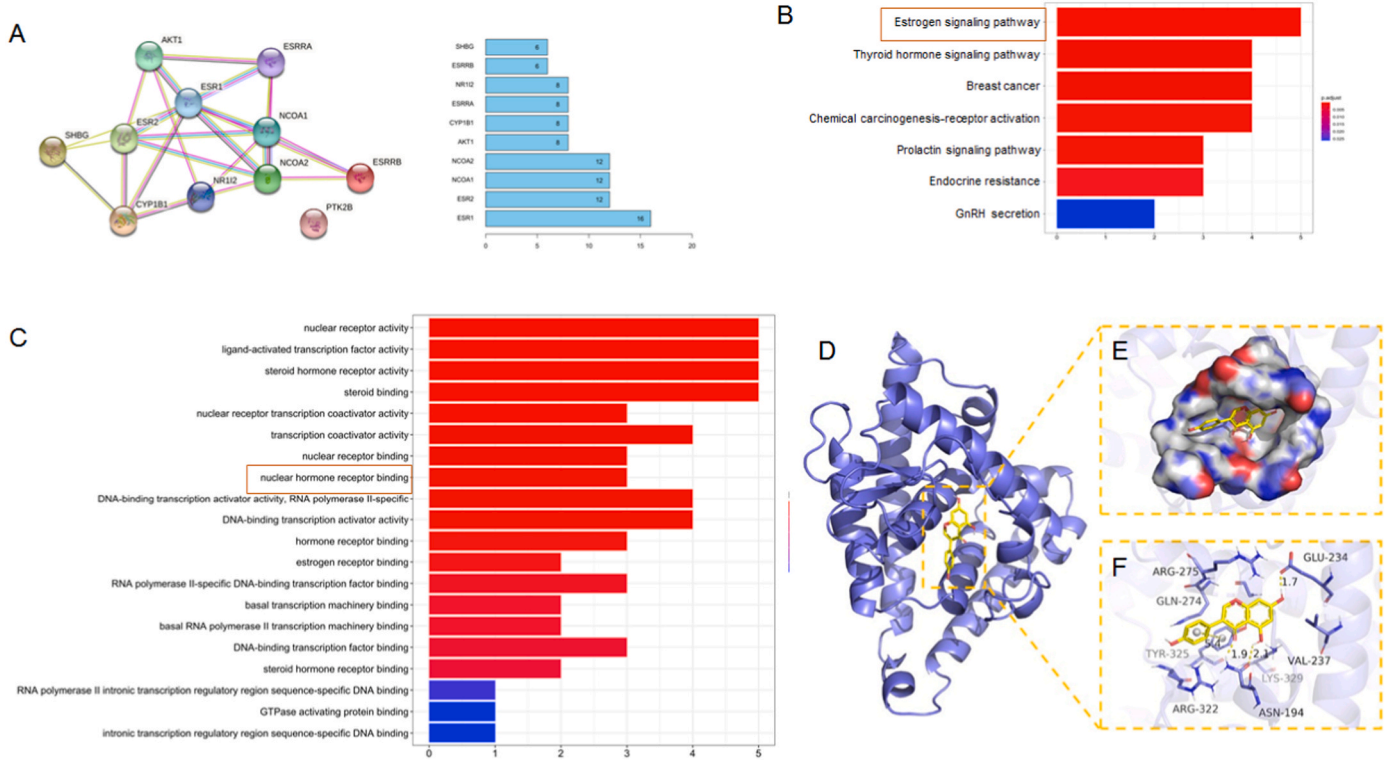

Fig. 4. The results of integrated bioinformatic analysis of genistein in postmenopausal osteoporosis (PMOP). (A) The protein-protein interaction (PPI) network of 11 primary genistein target proteins in PMOP. (B) KEGG analysis of the key targets of genistein. (C) GO enrichment analysis of the key targets of genistein. (D) The 3D structure of complex. (E) The surface of active site. (F) The detail binding mode of complex (The backbone of protein was rendered in tube and colored in blue, and genistein is rendering by yellow. Yellow dash represents hydrogen bond distance or π-stacking). (For interpretation of the references to color in this figure legend, the reader is referred to the Web version of this article.)

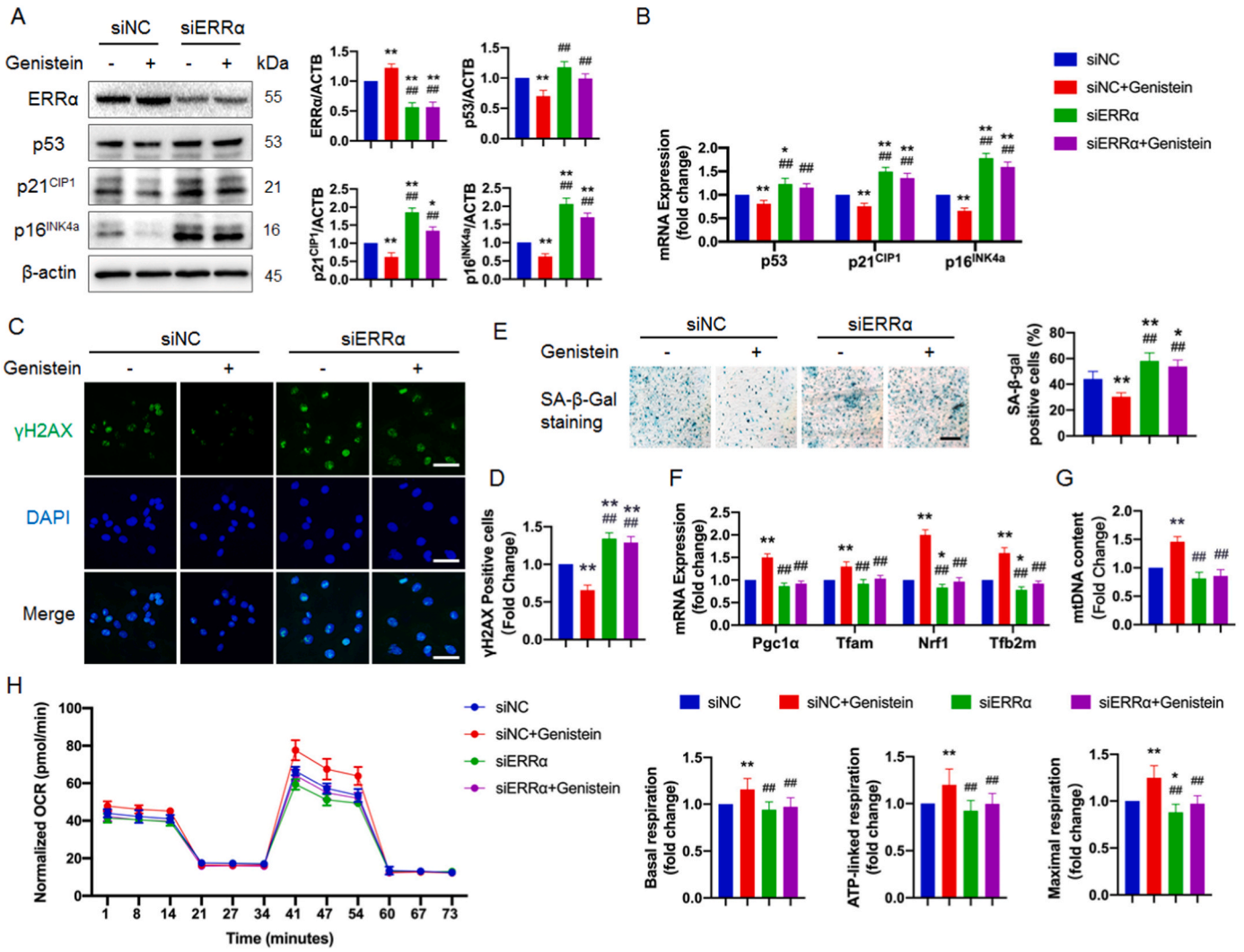

Fig. 5. Genistein attenuated senescence, promoted mitochondria biogenesis and autophagy via ERRα. OVX-BMMSCs were transfected with ERRα siRNA or control siRNA for 48 h and then cultured with 10^{-2} μM genistein for another 3 days. (A) Protein levels of ERRα, p53, $p16^{INK4a}$ and $p21^{CIP1}$ and representative blots (n = 3). β-actin was used as loading control. (B) The mRNA expression of senescence related marker p53, $p16^{INK4a}$ and $p21^{CIP1}$ in different groups (n = 3). (C, D) Representative images of γH2AX staining and quantitative assessment of the γH2AX positive cells (n = 3). Scale bar, 50 μm. (E) Representative images of SA-β-gal staining and quantitative assessment of the SA-β-gal positive cells (n = 3). Scale bar, 500 μm. (F) The mRNA expression of Pgc1α, Tfam, Nrf1 and Tfb2m in different groups (n = 3). (G) The mtDNA copy number was measured in each group (n = 3). (H) Oxygen-consumption rates (OCRs) of cells at baseline and in response to oligomycin A, FCCP, and rotenone plus antimycin A. Basal respiration, ATP-linked respiration and maximal respiration were shown on the right. Data show mean ± SD of three independent experiments from 3 rats. Significance was calculated using a one-way ANOVA followed by the Tukey's post-hoc test (A, B, D, E, F, G and H). *p < 0.05 and **p < 0.01 compared to the siNC + Control group. #p < 0.05 and ##p < 0.01 compared to the siNC + genistein group.

genistein were greatly attenuated by ERRα knockdown. The results of γH2AX immunofluorescence and SA-β-gal staining also showed that the inhibitory effect of genistein on cellular senescence was abrogated by knockdown of ERRα (Fig. 5C–E). We next analyzed the expression levels of mitochondrial biogenesis regulators and mitochondrial DNA copy number (mtDNA). The results showed that ERRα knockdown attenuated the effect of genistein to upregulate mRNA levels of mitochondrial biogenesis regulators and mtDNA (Fig. 5F and G). Parameters of mitochondrial respiration, including basal respiration, ATP-linked respiration, and maximum respiration, were significantly upregulated by genistein treatment (Fig. 5H). This effect was inhibited by ERRα knockdown (Fig. 5H), suggesting that the increase in mitochondrial respiration was depended on ERRα activity.

Functionally, treatment with ERRα siRNA attenuated the ability of genistein to reduce cellular and mitochondrial ROS level, as shown by the increase in ROS and MitoSOX fluorescence intensity (Fig. 6A–D). Knockdown of ERRα in OVX-BMMSCs also abolished the upregulation effect of genistein on mitochondrial membrane potential (Fig. 6E and F) and ATP production (Fig. 6G). Mitophagy is critical for maintaining normal mitochondria quality and quantity [23]. To investigate the involvement of ERRα in the genistein-induced mitophagy, we performed the MitoTracker Green (MTG, a dye that stain the mitochondria independent of membrane potential) and LysoTracker Red (LTR) co-staining. Mitophagy was enhanced by genistein treatment, as indicated by enhanced co-localization of MTG and LTR fluorescence (Fig. 6H, white arrowhead). However, ERRα knockdown markedly reduced the MTG and LTR co-localization (Fig. 6H and I). During canonical Parkin-mediated mitophagy, the activated PTEN-induced kinase protein 1 (Pink1) recruits cytosolic Parkin to the mitochondrial outer membrane and thus initiates mitophagy [24]. Sirtuin 3 (SIRT3), which can be upregulated by ERRα [22], plays an important role in the regulation of mitophagy by controlling the activity of Pink1 [25–27]. As shown in Fig. 6J and K, genistein upregulated SIRT3 expression, and promoted Parkin translocation to the mitochondria. Conversely, genistein-induced

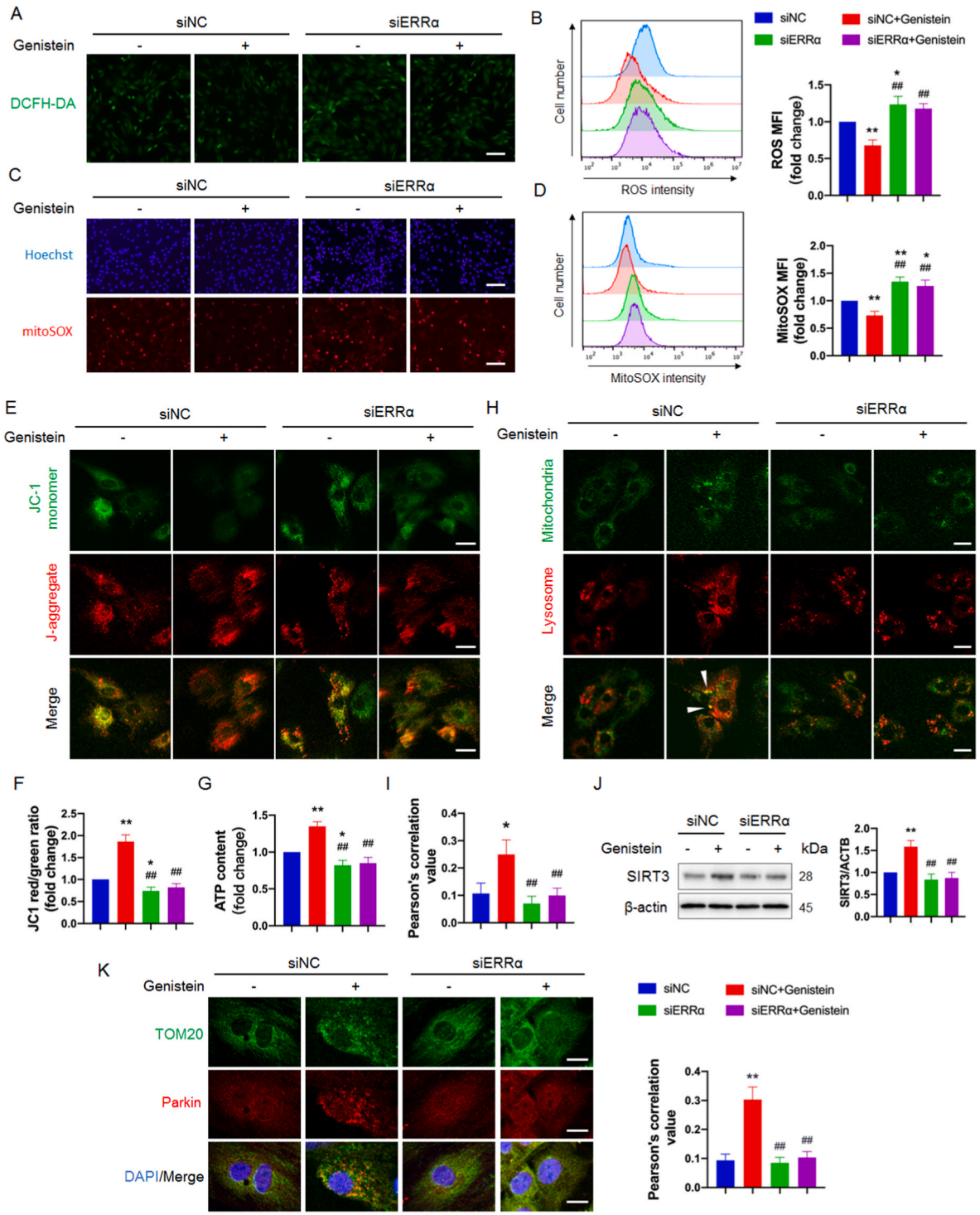

Fig. 6. Genistein attenuated oxidative stress and mitochondrial dysfunction, promoted mitophagy in an ERRα-dependent manner. OVX-BMMSCs were transfected with ERRα siRNA or control siRNA for 48 h and then stimulated with 10^{-2} μM genistein for 3 days (A, B, C, D, E, F, G and J) or 2 days (H, I and K). (A, B) Representative images and flow cytometric analysis of ROS level (n = 3). The MFI of siNC + Control group was normalized to 100%. Scale bar, 200 μm. (C, D) Flow cytometry of MitoSOX in different groups (n = 3). The MFI of siNC + Control group was normalized to 100%. (E, F) Representative images and flow cytometric analysis of JC-1 staining (n = 3). The JC1 red/green ratio of siNC + Control group were normalized to 100%. Scale bar, 25 μm. (G) The ATP level was measured and normalized to the protein amounts of cells (n = 3). The values of siNC + Control group were normalized to 100%. (H, I) Representative images of lysosomes labeled with red (LysoTracker Red, LTR) and mitochondria labeled with green (MitoTracker Green, MTG). Co-localization of both signals is counted as a mitophagy event (white arrowhead). Statistical evaluation is performed by calculating the Pearson's coefficient for colocalization of MTG and LTR. Scale bar, 20 μm. (J) Protein levels of SIRT3 were analyzed by western blots using β-actin as loading control (n = 3). (K) Representative images of cells stained with anti-TOM20 and anti-Parkin. The Pearson's coefficient between red and green fluorescence intensities were determined in 9 cells from three independent experiments. Scale bar, 10 μm. Values represent the mean ± SD of three independent experiments. Significance was calculated using a one-way ANOVA followed by the Tukey's post-hoc test (B, D, F, G, I, J and K). *p < 0.05 and **p < 0.01 compared to the siNC + Control group. #p < 0.05 and ##p < 0.01 compared to the siNC + genistein group. (For interpretation of the references to color in this figure legend, the reader is referred to the Web version of this article.)

SIRT3 upregulation were largely inhibited by transfection of siERRα (Fig. 6J), and Parkin retained its cytosolic distribution in ERRα-knockdown cells (Fig. 6K). These results confirmed that ERRα is required for the genistein-induced mitophagy.

Together, these results suggested that genistein attenuated estrogen deficiency induced cellular senescence and mitochondrial dysfunction in an ERRα-dependent manner.

3.6. Genistein inhibited bone loss and alleviated oxidative damage in OVX rats

Since our data showed that genistein protect BMMSCs from estrogen deficiency induced premature senescence, we tested whether genistein could protect ovariectomy-induced bone loss in rats. At post-operative 16-week, the OVX groups have significantly elevated serum levels of lipid peroxidation marker malondialdehyde (MDA) over the Sham groups (Fig. 7A). Genistein significantly decreased the MDA level over the OVX + VEH group ($p < 0.01$) (Fig. 7A).

Sendur et al. [28]. confirmed a negative correlation between plasma lipid oxidation and BMD values in osteoporotic postmenopausal women compared with a healthy group. Micro-CT 3D reconstruction images of proximal tibia demonstrated a significant trabecular bone loss in rats underwent ovariectomy, and eight weeks of genistein treatment significantly inhibited ovariectomy-induced bone loss (Fig. 7B). Further analysis on the parameters of trabecular bone revealed that ovariectomy led to trabecular bone microarchitecture deterioration in rats, as indicated by the decrease of BMD ($p < 0.01$), BV/TV ($p < 0.01$) and Tb.Th ($p < 0.01$), as well as the increase of Tb.Sp ($p < 0.01$). However, the administration of genistein ameliorated the deterioration of trabecular bone in the tibia of OVX rats (Fig. 7C). Compared to the Sham groups, bone strength of mid-femur and femoral head was significantly lower in OVX groups (Fig. 7D). Genistein treatment reversed the decrease of mid-femur peak load in OVX rats (Fig. 7D).

Bone histology also demonstrated the beneficial effect of genistein in ovariectomy-induced osteoporosis. Histology of the proximal tibia in OVX groups showed thin and sparse trabecular bone. Genistein treatment restored the architecture of trabecular bone in the OVX group (Fig. 7E). Estrogen deficiency markedly enhanced the expression of senescence related marker $p16^{INK4a}$ in the marrow cavity (Fig. 8A and B). Remarkably, genistein treatment substantially inhibited the $p16^{INK4a}$ positive staining in OVX groups (Fig. 8A and B). Moreover, the protein level of SIRT3 in bone marrow area of proximal tibia was significantly lower in OVX + VEH group versus Sham groups, and genistein treatment partially but significantly restored the SIRT3 expression (Fig. 8C and D). To investigate the PGC1α expression of MSCs in vivo, we performed PGC1α and LepR co-staining in the trabecular bone area of proximal tibia sections. It is well known that MSCs in adult bone marrow specifically express the leptin receptor (LepR) [29]. Double immunofluorescence labeling revealed that the number of $LepR^{+}$ cells positive for PGC1α in Sham groups were significantly higher than the OVX groups

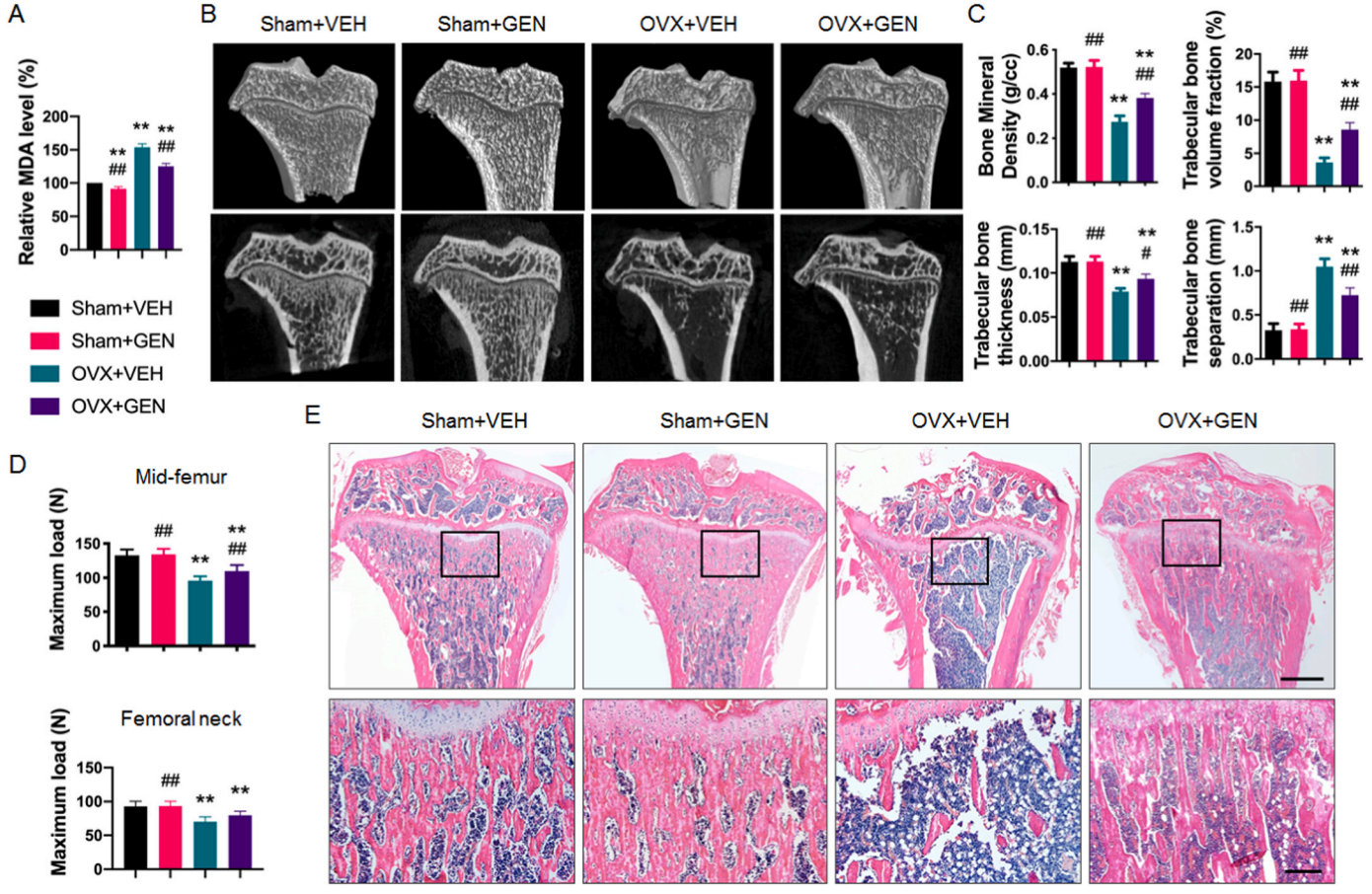

Fig. 7. Genistein alleviated serum oxidative damage and trabecular bone loss in ovariectomized rats. (A) Serum levels of malondialdehyde (MDA) in Sham + VEH, Sham + GEN, OVX + VEH and OVX + GEN groups (n = 15). (B) Representative micro-CT 3D (top) and 2D (bottom) images of proximal tibia in each group. (C) Bone histomorphometric analysis of total bone mineral dansity (BMD, g/cc), trabecular bone volume (BV/TV, %), trabecular thickness (Tb.Th, mm) and trabecular separation (Tb.Sp, mm) in the trabecular bone area (n = 9). (D) Maximum load of mid-femur and femoral neck in each group (n = 15). (E) Hematoxylin/eosin (HE) staining of the proximal tibia in different groups, images are representative photos of 9 proximal tibias. Upper scale bar, 1 mm. Lower scale bar, 200 μM. Each value is mean ± SD. Significance was calculated using a one-way ANOVA followed by the Tukey's post-hoc test (A, C and D). *$p < 0.05$ and **$p < 0.01$ compared to the Sham + VEH group. #$p < 0.05$ and ##$p < 0.01$ compared to the OVX + VEH group.

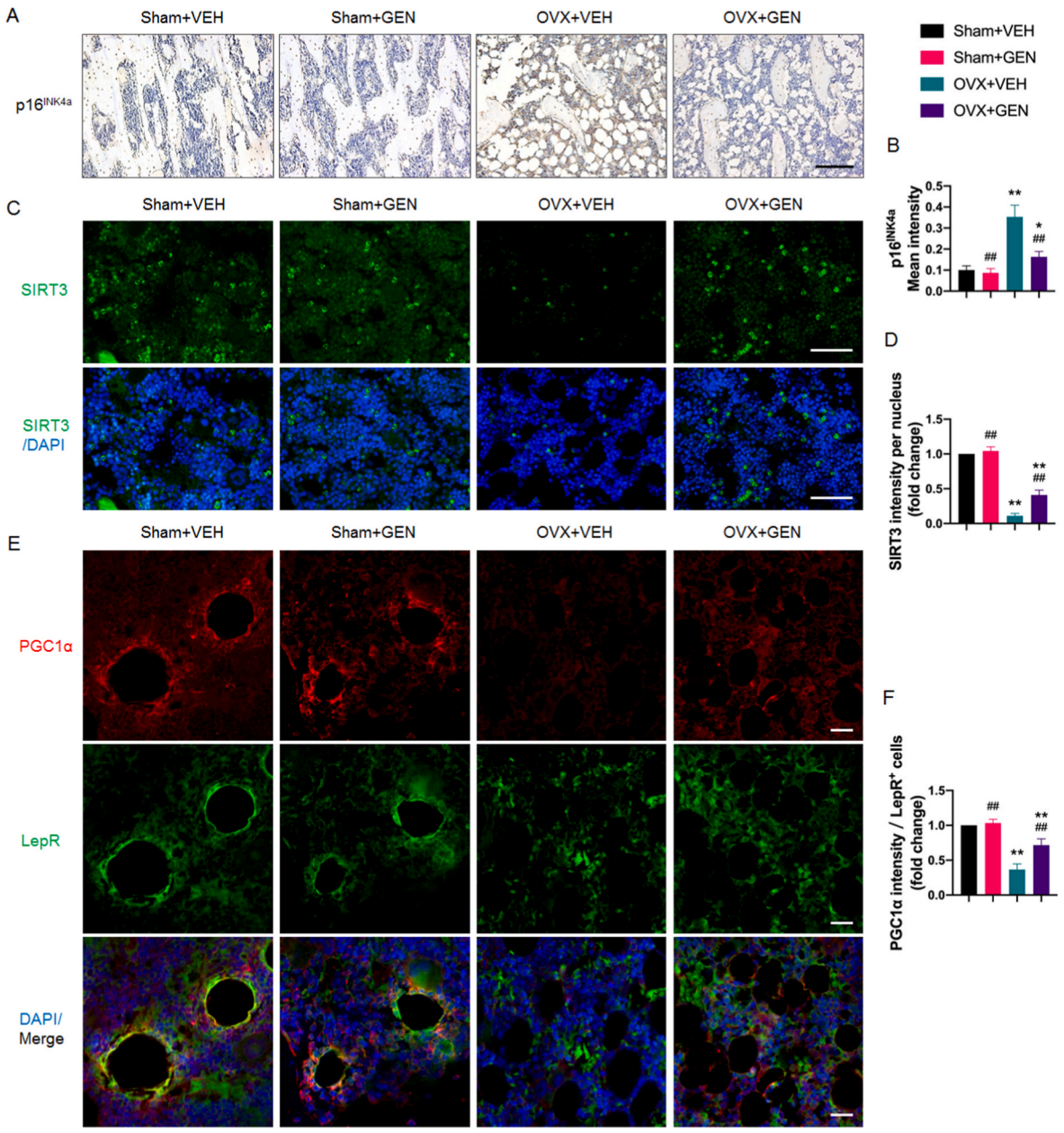

Fig. 8. Genistein treatment inhibited senescence marker $p16^{INK4a}$ expression and induced SIRT3 and PGC1α expression in the trabecular bone area of proximal tibia in ovariectomized rats. (A, B) Representative images of immunohistochemical staining of $p16^{INK4a}$ in different groups. Scale bar, 100 μM. The graph on the right showed mean intensity of $p16^{INK4a}$ staining (n = 9). (C, D) Representative images of immunofluorescence staining of SIRT3 (green) and nucleus (blue) in different groups. Scale bar, 50 μM. The graph on the right showed SIRT3 fluorescence intensity per nucleus, and the values of Sham + VEH group were normalized to 100% (n = 9). (E, F) Representative images of double immunofluorescence labeling of PGC1α and LepR at the bone marrow area of proximal tibia. Scale bar, 20 μM. The graph on the right showed PGC1α fluorescence intensity per $LepR^+$ cells, and the values of Sham + VEH group were normalized to 100% (n = 9). Each value is mean ± SD. Significance was calculated using a one-way ANOVA followed by the Tukey's post-hoc test (B, D and F). *p < 0.05 and **p < 0.01 compared to the Sham + VEH group. #p < 0.05 and ##p < 0.01 compared to the OVX + VEH group. (For interpretation of the references to color in this figure legend, the reader is referred to the Web version of this article.)

(Fig. 8E and F). Genistein treatment markedly upregulated the PGC1α expression in $LepR^+$ cells in the tibias of OVX rats (Fig. 8E and F). Together, these data provide in vivo evidence that genistein inhibited estrogen deficiency-induced premature senescence and upregulated SIRT3 and PGC1α expression in the trabecular bone area of OVX rats.

4. Discussion

Adult stem cells are essential for tissue maintenance and regeneration yet are susceptible to senescence during stress. Estrogen deficiency induces oxidative stress and impairs bone antioxidant system [30], leads to premature senescence of BMMSCs. Changes in the behavior of senescent BMMSCs include loss of potential to proliferate and differentiate in vitro, and loss of capacity to form bone in vivo. These changes are accounted for, at least in part, the development of PMOP. This study suggested for the first time that genistein mitigated premature senescence of OVX-BMMSCs through restoring mitochondrial homeostasis in an ERRα-dependent manner.

Mitochondrial dysfunctions, in particular bioenergetic decline and ROS accumulation, are crucial mechanisms underlying stem cell

senescence. Although stem cells rely predominantly on glycolysis for energy, mitochondrial function and homeostasis take pivotal roles in stem cell energy metabolism [31,32]. Low cellular ATP content caused by mitochondrial dysfunction eventually results in p53 activation and cell cycle arrest. Consistent with previous study [33], we found that OVX-BMMSCs presented premature senescence phenotype compared to Sham-BMMSCs. Further, increased cellular ROS level and mitochondrial-derived superoxide generation level, as well as reduced mitochondrial membrane potential and ATP content were found in OVX-BMMSCs, in accordance with the changes during stem cells aging [34]. Previous published studies have reported that genistein have mitochondria protecting effect in neurons through nuclear factor-κB signaling pathway [35,36]. We also found genistein could restore mitochondrial function in OVX-BMMSCs.

The mitochondrial homeostasis of stem cells is dependent on the overall quality and relative abundance of the mitochondrial population, which is determined by mitochondrial biogenesis and degradation. As Rasbach et al. [37] have reported that genistein could enhance mitochondrial biogenesis, we also found that genistein upregulated the expression of mitochondrial membrane proteins in OVX-BMMSCs. The biogenesis of mitochondrial is regulated by a large number of transcription factors and related regulatory proteins. Among these regulators, PGC1α,nuclear respiratory factors (Nrf1 and Nrf2), transcription factor A mitochondrial (Tfam) and transcription factor B2 mitochondrial (Tfb2m) play crucial roles in the context of mitochondrial biogenesis [38]. Mitochondrial DNA replication is initiated by Tfam, which is regulated by PGC1α and Nrf1. The elevated levels of PGC1α, Nrf1, Tfam and Tfb2m indicated that genistein promoted mitochondrial biogenesis through upregulation of these transcription factors.

Mitochondrial biogenesis must be coupled with control mechanisms such as mitophagy to maintain mitochondrial quality. Mitophagy is essential for maintaining stemness and preventing senescence in stem cells, as it specifically degrades damaged mitochondria, thereby reduces the source of ROS and inhibits ROS-induced DNA damage [39]. Besides directly impairs mitochondrial DNA, oxidative stress also impairs lysosomal function, leads to autophagic flux inhibition [40–42]. Among all cellular organelles, mitochondria and lysosomes undergo the most marked senescence-related alterations. In TEM images, we observed accumulation of large lysosomes in OVX-BMMSCs, indicating the incapability of lysosome turnover. Lysosome dysfunction hampers degradation of mitochondria, leading to increased ROS production, which in turn impairs lysosomes. This vicious circle between lysosomes and ROS thus aggravates cell senescence. We observed increased lysosomes fluorescence signal (Fig. 6H) and downregulated P62 level (Fig. 3F) in genistein-treated cells, suggesting that lysosome biogenesis and cargo processing were enhanced by genistein treatment. Our results are in line with the literatures which also reported that genistein was able to promote lysosome biogenesis and lysosomal metabolism [43,44]. Consequently, genistein enhanced mitophagy in OVX-BMMSCs, as shown by the result of TEM, western blot and live cell imaging microscopy (Fig. 3E, F, 6H and 6K).

It is well-known that genistein binds to estrogen receptor (ER) α and β and has ER-mediated estrogenic effects. However, it has anti-estrogenic effects as well as non-ER-mediated effects such as inhibition of tyrosine kinase [45]. Because of its complex biological actions, the molecular mechanisms of action of genistein remain elusive. Estrogen-related receptor alpha (ERRα) is a constitutive active ligand-independent orphan nuclear receptor belonging to the nuclear receptor superfamily. Although it shares a high amino acid sequence homology with estrogen receptors (ERs), estrogens are not ligands of ERRα [22]. Structure-function studies have revealed that genistein behaves as an agonist of ERRα [46]. Similarly, we also identified ERRα as a possible target protein which has a good binding effect with high matching degree with genistein. Huang et al. found that the expressions of PGC1α and ERRα are decreased in BMMSCs from aged mice, and compensation of ERRα rescues the osteogenic capability of elderly mouse BMMSCs in vitro [47], which indicates that the PGC1α and ERRα play important roles in BMMSC senescence. Numerous studies have reported that ERRα is a key effector in the regulation of PGC1α-dependent transcripts involved in mitochondrial biogenesis and function [48–50]. Interestingly, ERRα and PGC1α often show similar expression profiles in tissues [47,51]. PGC1α has structural motifs specific for binding to ERRα, and the PGC1α-ERRα complex upregulates the expression of ERRα in a feed-forward manner. Ligand of ERRα upregulates expression of PGC1α in an ERRα-dependent manner [52]. Inhibition of ERRα impairs the ability of PGC1α to enhance mitochondrial gene expression in thyroid cell lines [53]. Our study also found that knockdown of ERRα abolished the inducing effect of genistein on PGC1α (Fig. 5A and B). Consequently, genistein upregulated expressions of mitochondria biogenesis transcription factors, mitochondria DNA copy number and oxygen consumption rate were inhibited by siERRα (Fig. 5F, G and H). SIRT3, one member of the sirtuins family, is responsible for deacetylation of mitochondrial proteins and modulation of mitophagy [12]. Studies have found that SIRT3 directly deacetylate PINK1, thus activates PINK1 and recruits Parkin from cytosol to mitochondria to ubiquitinate the outer mitochondrial membrane proteins, which serves as a “eat-me” signal for ultimate mitophagy [26,27,54]. ERRα is known to bind the proximal SIRT3 gene promoter region and thus promotes SIRT3 expression [55]. As shown in Fig. 6J and K, genistein-induced SIRT3 expression and TOM20-Parkin co-localization were significantly inhibited by ERRα knockdown. Live cell imaging microscopy also showed that siRNA against ERRα greatly attenuated genistein-induced mitophagy (Fig. 6H).

Collectively, these findings showed that the coordinated increase in mitochondrial turnover through biogenesis and mitophagy by genistein was ERRα-dependent. It also suggests that ERRα is a potentially therapeutic target to counteract bone loss in PMOP.

5. Conclusions

Taken together, our results demonstrate that estrogen deficiency led to the impaired mitochondrial function and premature senescence of BMMSCs. Genistein exerts anti-senescence effect on OVX-BMMSCs by restoring mitochondrial homeostasis via ERRα, which provide further evidence for its use as a natural compound for treating postmenopausal osteoporosis. It also validates ERRα as a promising target for the development of therapeutic interventions on PMOP.

Author contributions

MYL and YJY performed most of the experiments. KX prepared the bone specimens and performed the histology. JYL and GHS generated the OVX rat model. JJW performed the immunofluorescence staining. WTQ and SYW contributed to analysis and interpretation of data. JWZ and CY supervised the study, and revised manuscript critically for important intellectual content. JG designed the experiments and wrote the manuscript. All authors have read and approved the manuscript.

Funding

This study was supported by the National Natural Science Foundation of China (grant number, 32000976 and 82071134).

Declaration of competing interest

The authors declare no competing interests.

Data availability

Data will be made available on request.

Acknowledgements

We thank all authors for commenting on the manuscript.

Appendix A. Supplementary data

Supplementary data to this article can be found online at https://doi.org/10.1016/j.redox.2023.102649.

References

[1] K.E. Ensrud, C.J. Crandall, Osteoporosis, Ann. Intern. Med. 167 (2017) Itc17–itc32.
[2] G. Kasper, L. Mao, S. Geissler, A. Draycheva, J. Trippens, J. Kühnisch, et al., Insights into mesenchymal stem cell aging: involvement of antioxidant defense and actin cytoskeleton, Stem Cell. 27 (2009) 1288–1297.
[3] C.X. Zheng, B.D. Sui, X.Y. Qiu, C.H. Hu, Y. Jin, Mitochondrial regulation of stem cells in bone homeostasis, Trends Mol. Med. 26 (2020) 89–104.
[4] J.H. An, J.Y. Yang, B.Y. Ahn, S.W. Cho, J.Y. Jung, H.Y. Cho, et al., Enhanced mitochondrial biogenesis contributes to Wnt induced osteoblastic differentiation of C3H10T1/2 cells, Bone 47 (2010) 140–150.
[5] G. Lou, K. Palikaras, S. Lautrup, M. Scheibye-Knudsen, N. Tavernarakis, E.F. Fang, Mitophagy and neuroprotection, Trends Mol. Med. 26 (2020) 8–20.
[6] R. Singh, S. Kaushik, Y. Wang, Y. Xiang, I. Novak, M. Komatsu, et al., Autophagy regulates lipid metabolism, Nature 458 (2009) 1131–1135.
[7] Y.H. Yang, B. Li, X.F. Zheng, J.W. Chen, K. Chen, S.D. Jiang, et al., Oxidative damage to osteoblasts can be alleviated by early autophagy through the endoplasmic reticulum stress pathway–implications for the treatment of osteoporosis, Free Radic. Biol. Med. 77 (2014) 10–20.
[8] H. Marini, L. Minutoli, F. Polito, A. Bitto, D. Altavilla, M. Atteritano, et al., Effects of the phytoestrogen genistein on bone metabolism in osteopenic postmenopausal women: a randomized trial, Ann. Intern. Med. 146 (2007) 839–847.
[9] A. Bitto, H. Marini, B.P. Burnett, F. Polito, R.M. Levy, N. Irrera, et al., Genistein aglycone effect on bone loss is not enhanced by supplemental calcium and vitamin D3: a dose ranging experimental study, Phytomedicine 18 (2011) 879–886.
[10] L.L. Legette, W.H. Lee, B.R. Martin, J.A. Story, A. Arabshahi, S. Barnes, et al., Genistein, a phytoestrogen, improves total cholesterol, and Synergy, a prebiotic, improves calcium utilization, but there were no synergistic effects, Menopause 18 (2011) 923–931.
[11] M.A. Rahman, M.H. Rahman, P. Biswas, M.S. Hossain, R. Islam, M.A. Hannan, et al., Potential therapeutic role of phytochemicals to mitigate mitochondrial dysfunctions in alzheimer's disease, Antioxidants 10 (2020).
[12] D.J. Klionsky, A.K. Abdel-Aziz, S. Abdelfatah, M. Abdellatif, A. Abdoli, S. Abel, et al., in: Guidelines for the use and interpretation of assays for monitoring autophagy, (4th edition)(1) 17, 2021, pp. 1–382. Autophagy.
[13] N. Manzella, Y. Santin, D. Maggiorani, H. Martini, V. Douin-Echinard, J.F. Passos, et al., Monoamine oxidase-A is a novel driver of stress-induced premature senescence through inhibition of parkin-mediated mitophagy, Aging Cell 17 (2018), e12811.
[14] K.I. Korski, D.A. Kubli, B.J. Wang, F.G. Khalafalla, M.M. Monsanto, F. Firouzi, et al., Hypoxia prevents mitochondrial dysfunction and senescence in human c-kit(+) cardiac progenitor cells, Stem Cell. 37 (2019) 555–567.
[15] M. Li, Y. Yu, Y. Shi, Y. Zhou, W. Zhang, H. Hua, et al., Decreased osteogenic ability of periodontal ligament stem cells leading to impaired periodontal tissue repair in BRONJ patients, Stem Cell. Dev. 29 (2020) 156–168.
[16] M. Rajeswari, N. Santhi, V. Bhuvaneswari, Pharmacophore and virtual screening of JAK3 inhibitors, Bioinformation 10 (2014) 157–163.
[17] R. Fazi, C. Tintori, A. Brai, L. Botta, M. Selvaraj, A. Garbelli, et al., Homology model-based virtual screening for the identification of human helicase DDX3 inhibitors, J. Chem. Inf. Model. 55 (2015) 2443–2454.
[18] Y.L. Ma, M. Hamang, J. Lucchesi, N. Bivi, Q. Zeng, M.D. Adrian, et al., Time course of disassociation of bone formation signals with bone mass and bone strength in sclerostin antibody treated ovariectomized rats, Bone 97 (2017) 20–28.
[19] M. Heim, O. Frank, G. Kampmann, N. Sochocky, T. Pennimpede, P. Fuchs, et al., The phytoestrogen genistein enhances osteogenesis and represses adipogenic differentiation of human primary bone marrow stromal cells, Endocrinology 145 (2004) 848–859.
[20] S.R. Hough, I. Clements, P.J. Welch, K.A. Wiederholt, Differentiation of mouse embryonic stem cells after RNA interference-mediated silencing of OCT4 and Nanog, Stem Cell. 24 (2006) 1467–1475.
[21] S.C. Manolagas, From estrogen-centric to aging and oxidative stress: a revised perspective of the pathogenesis of osteoporosis, Endocr. Rev. 31 (2010) 266–300.
[22] M. Tripathi, P.M. Yen, B.K. Singh, Estrogen-related receptor alpha: an under-appreciated potential target for the treatment of metabolic diseases, Int. J. Mol. Sci. 21 (2020).
[23] L. Garcia-Prat, M. Martinez-Vicente, E. Perdiguero, L. Ortet, J. Rodriguez-Ubreva, E. Rebollo, et al., Autophagy maintains stemness by preventing senescence, Nature 529 (2016) 37–42.
[24] M. Lazarou, D.A. Sliter, L.A. Kane, S.A. Sarraf, C. Wang, J.L. Burman, et al., The ubiquitin kinase PINK1 recruits autophagy receptors to induce mitophagy, Nature 524 (2015) 309–314.
[25] T. Wei, G. Huang, J. Gao, C. Huang, M. Sun, J. Wu, et al., Sirtuin 3 deficiency accelerates hypertensive cardiac remodeling by impairing angiogenesis, J. Am. Heart Assoc. 6 (2017).
[26] L. Wang, H. Qi, Y. Tang, H.M. Shen, Post-translational modifications of key machinery in the control of mitophagy, Trends Biochem. Sci. 45 (2020) 58–75.
[27] W. Ling, K. Krager, K.K. Richardson, A.D. Warren, F. Ponte, N. Aykin-Burns, et al., Mitochondrial Sirt3 contributes to the bone loss caused by aging or estrogen deficiency, JCI Insight (2021) 6.
[28] O.F. Sendur, Y. Turan, E. Tastaban, M. Serter, Antioxidant status in patients with osteoporosis: a controlled study, Joint Bone Spine 76 (2009) 514–518.
[29] B.O. Zhou, R. Yue, M.M. Murphy, J.G. Peyer, S.J. Morrison, Leptin-receptor-expressing mesenchymal stromal cells represent the main source of bone formed by adult bone marrow, Cell Stem Cell 15 (2014) 154–168.
[30] S. Muthusami, I. Ramachandran, B. Muthusamy, G. Vasudevan, V. Prabhu, V. Subramaniam, et al., Ovariectomy induces oxidative stress and impairs bone antioxidant system in adult rats, Clin. Chim. Acta 360 (2005) 81–86.
[31] N. Sun, R.J. Youle, T. Finkel, The mitochondrial basis of aging, Mol. Cell 61 (2016) 654–666.
[32] P.R. Angelova, M. Barilani, C. Lovejoy, M. Dossena, M. Vigano, A. Seresini, et al., Mitochondrial dysfunction in Parkinsonian mesenchymal stem cells impairs differentiation, Redox Biol. 14 (2018) 474–484.
[33] W. Wu, J. Fu, Y. Gu, Y. Wei, P. Ma, J. Wu, JAK2/STAT3 regulates estrogen-related senescence of bone marrow stem cells, J. Endocrinol. 245 (2020) 141–153.
[34] Z.D. Hao, S. Liu, Y. Wu, P.C. Wan, M.S. Cui, H. Chen, et al., Abnormal changes in mitochondria, lipid droplets, ATP and glutathione content, and Ca(2+) release after electro-activation contribute to poor developmental competence of porcine oocyte during in vitro ageing, Reprod. Fertil. Dev. 21 (2009) 323–332.
[35] S.L. Valles, C. Borras, J. Gambini, J. Furriol, A. Ortega, J. Sastre, et al., Oestradiol or genistein rescues neurons from amyloid beta-induced cell death by inhibiting activation of p38, Aging Cell 7 (2008) 112–118.
[36] Y. Qian, T. Guan, M. Huang, L. Cao, Y. Li, H. Cheng, et al., Neuroprotection by the soy isoflavone, genistein, via inhibition of mitochondria-dependent apoptosis pathways and reactive oxygen induced-NF-kappaB activation in a cerebral ischemia mouse model, Neurochem. Int. 60 (2012) 759–767.
[37] K.A. Rasbach, R.G. Schnellmann, Isoflavones promote mitochondrial biogenesis, J. Pharmacol. Exp. Therapeut. 325 (2008) 536–543.
[38] D. Wang, Y. Wang, X. Zou, Y. Shi, Q. Liu, T. Huyan, et al., FOXO1 inhibition prevents renal ischemia-reperfusion injury via cAMP-response element binding protein/PPAR-γ coactivator-1α-mediated mitochondrial biogenesis, Br. J. Pharmacol. 177 (2020) 432–448.
[39] H. Zhang, K.J. Menzies, J. Auwerx, The role of mitochondria in stem cell fate and aging, Development (2018) 145.
[40] C. Luo, Y. Li, H. Wang, Z. Feng, Y. Li, J. Long, et al., Mitochondrial accumulation under oxidative stress is due to defects in autophagy, J. Cell. Biochem. 114 (2013) 212–219.
[41] V.I. Korolchuk, S. Miwa, B. Carroll, T. von Zglinicki, Mitochondria in cell senescence: is mitophagy the weakest link? EBioMedicine 21 (2017) 7–13.
[42] H. Tai, Z. Wang, H. Gong, X. Han, J. Zhou, X. Wang, et al., Autophagy impairment with lysosomal and mitochondrial dysfunction is an important characteristic of oxidative stress-induced senescence, Autophagy 13 (2017) 99–113.
[43] M. Moskot, S. Montefusco, J. Jakobkiewicz-Banecka, P. Mozolewski, A. Wegrzyn, D. Di Bernardo, et al., The phytoestrogen genistein modulates lysosomal metabolism and transcription factor EB (TFEB) activation, J. Biol. Chem. 289 (2014) 17054–17069.
[44] L.R. Rega, E. Polishchuk, S. Montefusco, G. Napolitano, G. Tozzi, J. Zhang, et al., Activation of the transcription factor EB rescues lysosomal abnormalities in cystinotic kidney cells, Kidney Int. 89 (2016) 862–873.
[45] L.G. Ming, K.M. Chen, C.J. Xian, Functions and action mechanisms of flavonoids genistein and icariin in regulating bone remodeling, J. Cell. Physiol. 228 (2013) 513–521.
[46] M. Suetsugi, L. Su, K. Karlsberg, Y.C. Yuan, S. Chen, Flavone and isoflavone phytoestrogens are agonists of estrogen-related receptors, Mol. Cancer Res. 1 (2003) 981–991.
[47] T. Huang, R. Liu, X. Fu, D. Yao, M. Yang, Q. Liu, et al., Aging reduces an ERRalpha-directed mitochondrial glutaminase expression suppressing glutamine anaplerosis and osteogenic differentiation of mesenchymal stem cells, Stem Cell. 35 (2017) 411–424.
[48] B.K. Singh, R.A. Sinha, M. Tripathi, A. Mendoza, K. Ohba, J.A.C. Sy, et al., Thyroid hormone receptor and ERRα coordinately regulate mitochondrial fission, mitophagy, biogenesis, and function, Sci. Signal. 11 (2018).
[49] P. Dhillon, J. Park, C. Hurtado Del Pozo, L. Li, T. Doke, S. Huang, et al., The nuclear receptor ESRRA protects from kidney disease by coupling metabolism and differentiation, Cell Metabol. 33 (2021) 379–394, e378.
[50] S. Kim, J.Y. Lee, S.G. Shin, J.K. Kim, P. Silwal, Y.J. Kim, et al., ESRRA (estrogen related receptor alpha) is a critical regulator of intestinal homeostasis through activation of autophagic flux via gut microbiota, Autophagy 17 (2021) 2856–2875.
[51] Y. Cho, S. Tachibana, K. Lam, Y. Arita, S. Khosrowjerdi, O. Zhang, et al., Perm1 promotes cardiomyocyte mitochondrial biogenesis and protects against hypoxia/reoxygenation-induced damage in mice, J. Biol. Chem. 297 (2021), 100825.
[52] S.K. Dwivedi, N. Singh, R. Kumari, J.S. Mishra, S. Tripathi, P. Banerjee, et al., Bile acid receptor agonist GW4064 regulates PPARγ coactivator-1α expression through estrogen receptor-related receptor α, Mol. Endocrinol. 25 (2011) 922–932.
[53] D. Mirebeau-Prunier, S. Le Pennec, C. Jacques, N. Gueguen, J. Poirier, Y. Malthiery, et al., Estrogen-related receptor alpha and PGC-1-related coactivator

constitute a novel complex mediating the biogenesis of functional mitochondria, FEBS J. 277 (2010) 713–725.

[54] G. Li, Z. Jian, H. Wang, L. Xu, T. Zhang, J. Song, Irisin promotes osteogenesis by modulating oxidative stress and mitophagy through SIRT3 signaling under diabetic conditions, Oxid. Med. Cell. Longev. 2022 (2022), 3319056.

[55] A. Giralt, E. Hondares, J.A. Villena, F. Ribas, J. Díaz-Delfín, M. Giralt, et al., Peroxisome proliferator-activated receptor-gamma coactivator-1alpha controls transcription of the Sirt3 gene, an essential component of the thermogenic brown adipocyte phenotype, J. Biol. Chem. 286 (2011) 16958–16966.